
FLUID PROPERTY PREDICTION LEVERAGING AI AND ROBOTICS

A PREPRINT

Jong Hoon Park, Gauri Pramod Dalwankar, Alison Bartsch, Abraham George, and Amir Barati Farimani

Carnegie Mellon University

{jonghoop, gdalwank, abartsch, aigeorge}@andrew.cmu.edu, barati@cmu.edu

ABSTRACT

Inferring liquid properties from vision is a challenging task due to the complex nature of fluids, both in behavior and detection. Nevertheless, the ability to infer their properties directly from visual information is highly valuable for autonomous fluid handling systems, as cameras are readily available. Moreover, predicting fluid properties purely from vision can accelerate the process of fluid characterization saving considerable time and effort in various experimental environments. In this work, we present a purely vision-based approach to estimate viscosity, leveraging the fact that the behavior of the fluid oscillations is directly related to the viscosity. Specifically, we utilize a 3D convolutional autoencoder to learn latent representations of different fluid-oscillating patterns present in videos. We leverage this latent representation to visually infer the category of fluid or the dynamics viscosity of fluid from video.

1 Introduction

Viscosity is a fundamental property of fluids that plays an important role in numerous industrial applications such as product quality control [1, 2], engineering pump design [3], and food processing [4]. Conventionally, its measurement is achieved using viscometers or rheometers, which require a labor-intensive process. The experimenter must select an appropriate device based on the fluid under examination, and the measurement can be time-consuming depending on fluid type, temperature, and viscometer size [2]. To address those experimental challenges, there have been many recent approaches to exploit the automation capability of robots or vision-based systems in both industries and academic laboratories, which shows great potential to significantly alleviate the labor-intensive processes and time cost [5, 6, 7, 8, 9].

In the context of perceiving viscosities of different fluids, humans can intuitively *perceive* viscosities by observing the oscillation dynamics of fluids. Each fluid type exhibits a unique damping coefficient discernible in its oscillation pattern, and the decay rate offers a direct correlation to the viscosity of the fluid [10, 11]. For example, shaking a bottle with less viscous fluid would result in slower decay of oscillations, and vice versa. However, understanding these properties is inherently challenging for autonomous systems due to the non-rigid structures and complex behavior of fluids [10, 12, 13]. In robotics, interactive perception emphasizes the crucial role of physical interaction in perception tasks. It suggests that by physically engaging with the environment, robots can have access to more diverse data and make more accurate inferences about their surroundings than they could through passive observation alone [14, 15].

With the recent increase in machine learning-based fluid modeling [16, 17, 18, 19], robotic fluid handling [20, 21, 22, 23, 24] and laboratory-based robotic systems [25, 26, 27], we propose leveraging interactive perception to autonomously predict viscosity. Recently, a number of approaches such as Reduced-Order Modeling [28], Graph Neural Network-based modeling [16], and physics-informed modeling [18, 29] have made significant progress in modeling fluid dynamics and accelerating fluid simulations in Computational Fluid Dynamics (CFD). In contrast, our work presents a purely vision-based approach to perform **two** tasks that can allow the robot to learn the oscillation properties of different fluids from video data: **1)** classification of fluid types by analyzing videos of five different oscillating fluids and **2)** prediction of fluid viscosity from videos of oscillating glycerol solutions at eight different viscosity levels. Specifically, we harness the principles of interactive perception by enabling the Franka Emika Panda robot arm to generate oscillations in various fluid samples. This interactive approach not only automates the initiation of fluid oscil-

lations for the laborious video collection process but also provides consistent agitation to the fluid bottle throughout each recording. We attempt to extract features relevant to fluid oscillation from the videos by masking the fluid region using the pre-trained segmentation model,[30] which successfully segments transparent liquid inside a transparent container. Then we employ a 3D convolutional autoencoder architecture to learn the latent representations of different oscillation patterns by reconstructing the single-channel mask videos. Lastly, to perform the downstream tasks, we discard the decoder and attach the encoder to either a classification or regression head to make the final prediction on fluid category and viscosity respectively. The contributions of our work can be summarized into three-fold.

- We propose an interactive perception approach to understand oscillation patterns in fluids, which could significantly reduce the rigorous experimental efforts required for viscosity measurement.
- We propose a video-based 3D convolutional autoencoder to encode fluid oscillation patterns into latent representations, which can be transferred for downstream tasks such as fluid class prediction or viscosity regression.
- To the best of our knowledge, this paper is the first to investigate the relationship between fluid properties, specifically viscosity, and the oscillation patterns observed in videos.

2 Related Works

Interactive Perception: In robotics, interactive perception (IP) is an active field of research where robots physically interact with their environment to enhance their understanding and perception.[14] Traditional perception methods using passive sensor information are often insufficient to provide robots with a comprehensive understanding of their physical environment. IP can ground the sensor observations and provide the robot with an additional stream of information. Following the advances in machine learning, recent studies have shown promising results on various manipulation and perception tasks employing IP. In an earlier study, K. Hausman et al.[31] utilized information from IP with probabilistic models to reduce uncertainties in articulated motion models for different cabinet door configurations. By integrating visual sensing, physical interaction, and intelligent action selection, they demonstrate the robot’s ability to effectively handle a variety of articulation models in their task. Work by M. Baum et al.[32] utilized active learning in their work on opening a mechanical puzzle called the lockbox, interactively exploring the structures of various lockboxes. In M. A. Lee et al.,[33] the robot relies on multimodal information such as vision, depth, force-torque, and proprioception obtained through IP to perform robust peg insertion task and demonstrate the transferability of the multimodal latent space. Specifically, they perform self-

supervised representation learning on each of multimodal inputs followed by the deep reinforcement learning to find the optimal latent policy. In L. Shao et al.[15], the robot is provided with a deep neural network (DNN) to process the visual effect of its interaction to estimate the scene flow and segmentation masks from two consecutive RGB-D input images. Their IP approach on motion-based object segmentation in a cluttered environment were able to segment well for both the synthetic data and real-world data. More recent work of Shao et al. [34] introduces fixtures to the workspace which can be autonomously manipulated by the robot arm. The fixtures provide physical constraints for robot motion and facilitate the reinforcement learning of manipulation skills such as peg insertion, wrench manipulation, and shallow depth insertion.

Fluid Modeling and Property Prediction: Due to the importance of understanding the behaviors of different fluids and their properties, much work has focused on modeling fluid dynamics and estimating fluid properties. For modeling fluid dynamics, the works of P. Pranshu et al. [28] and D. Shu et al. [18] both aim to reduce the computational cost of Navier-Stokes equation-based fluid simulations in Computational Fluid Dynamics (CFD). In the works of Z. Li and A. B. Farimani [16], they propose Fluid Graph Networks (FGN) to provide a computationally efficient point-based fluid simulator while improving the accuracy and stability of incompressible fluid simulation. For vision-based approaches that fit more into the scope of our work, J. Assen et al. [12] train a deep neural network to predict fluid viscosity from image sequences of a simulation-based dataset of fluid splashing, pouring, and stirring. While this pipeline proved effective at predicting viscosity, the data is entirely collected from a simulation, which avoids many of the key challenges of handling real-world fluid data. The work of S. Kv and V. Shenoy [35] presents a vision-based pipeline for viscosity prediction leveraging the principle of dispersion of incident light. This is an interaction-free technique to estimate viscosity, as the dispersion of light is directly related to the fluid viscosity. They hand-design features to collect from the refracted images of different fluids and train a neural network to predict the viscosity from these features. While this method to predict viscosity is effective, it requires a very specific experimental setup. In H. J. Huang et al. [10], researchers propose a pipeline to predict viscosity through interaction by relating the force measurements when shaking a container of fluid to viscosity. Specifically, they leverage GelSight [36], a visuo-tactile sensor, to sense the force changes caused by the bulk fluid movement. They fit a Gaussian Process Regression model to estimate the liquid properties from these force signals.

Segmenting Transparent Fluids: Transparent object perception is a challenging task due to their different appearances inherited from the image background [37]. Despite the difficulties, it is necessary to build systems that can accurately segment transparent objects and fluids to be applied for various fluid-handling robotic/vision systems. J. Liao et al. [38] present an approach to segment

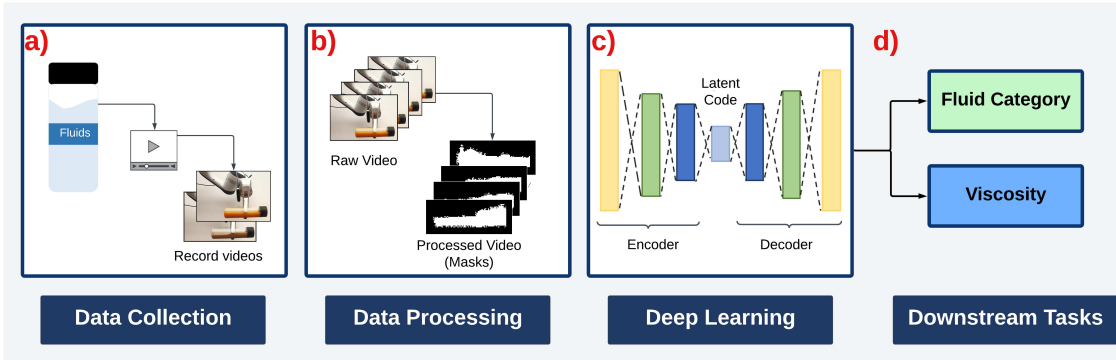


Figure 1: **Overview of the Fluid Learning Pipeline.** a) Oscillation videos of fluid samples are collected with the help of Franka Emika Panda arm to automate the collection process. b) Raw videos are transformed into segmentation masks with the frames focused on the fluid portion of the original ones. c) Processed input mask data are used to train the autoencoder. d) Latent codes learned by the autoencoder are transferred to use for fluid classification (green) and viscosity regression (blue) tasks.

transparent objects from video sequences, using trajectory clustering to distinguish the transparent object from the background, however this work focuses on transparent objects and cannot handle transparent liquid within the transparent vessel. In an early work addressing transparent fluid segmentation, A. Yamaguchi and C. G. Atkeson [39] use optical flow to detect fluid flow as liquid pours from source contained to target container. In the work of C. Schenck and D. Fox [40], they heat up the liquid and use a thermographic camera to accurately generate ground truth segmentation masks to train a model for the fluid-pouring task. However, this approach is not applicable for our work since ours require data collection at constant temperature to obtain accurate viscosity labels. Another previous approach in segmenting a transparent liquid by G. Narasimhan et al. [41] builds a Generative Adversarial Network (GAN) to convert RGB image of a liquid to transparent ones. This generative model is used to provide synthetic segmentation labels for the transparent liquids. They demonstrate the effectiveness of this vision pipeline by incorporating it into a robotic pouring task, which requires accurate estimation of the fluid quantity through visual inference. However, this system assumes relatively stationary liquid, and is not effective in our case where we consider fluid oscillation as valuable information. S. Eppel et al. [30] presents a model using modern computer vision methodologies to segment and classify medical fluid samples within transparent vessels. They employ a hierarchical, two-layer network to first segment the transparent vessels in the image, and subsequently segment the fluid within the vessels. The model was trained with the Vector-LabPics dataset which consists of 2,187 images of vessels and materials in chemistry lab settings and was used throughout this work for all fluid segmentation steps.

Video-Based Autoencoders: There are a number of studies that explore the use of autoencoders trained on video data for a variety of tasks. For instance, K. Wang et al. [42] proposed Video-Specific Autoencoders, a method that enables the editing and transmission of a single video

through latent space arithmetic. In contrast to our work, the Video-Specific Autoencoder consisted of 2D convolutional layers that encode each frame in the video to allow editing of a specific video. However, their use of Principal Component Analysis (PCA) for visualizing what the autoencoder was learning provided valuable insights, and a similar analysis was done in Section 5.2 of our study. In the work of Z. Lai et al. [43], the authors use self-supervised method that utilizes temporal continuity in videos to disentangle and learn representations of 3D structure and camera pose. The autoencoder extracts a temporally-consistent deep voxel feature for the 3D structure and a 3D trajectory for each frame’s camera pose, which can be re-entangled for rendering the video frames without the need for ground truth 3D or pose annotations. This method demonstrates its utility in tasks like novel view synthesis, camera pose estimation, and motion-following video generation evaluated on several large-scale natural video datasets. Another video-based autoencoder approach by Y. Chang et al. [44] employs a unique architecture that learns the spatial and temporal information separately using two autoencoders in parallel for anomaly detection, showing state-of-the-art performance on various video datasets.

3 Methods

In this section, we discuss the preprocessing steps applied to the raw videos and the deep learning pipelines. In Section 3.1, we briefly present the architecture of the segmentation model [30] and how the collected RGB videos are processed into a dataset of segmentation masks. In Section 3.2, we provide our procedures for training the 3D convolutional autoencoder with oscillation information. Lastly, in Section 3.3, we briefly discuss the respective methods applied for the downstream classification and regression tasks harnessing the pretrained autoencoder.

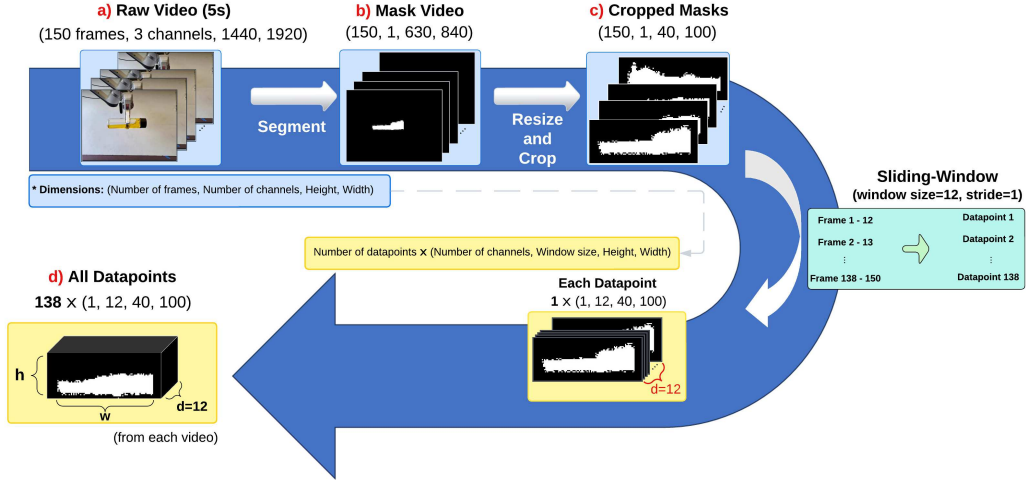


Figure 2: **Video Processing on Single Video.** a, b) Fluid oscillation in each frame of the raw video is masked via semantic segmentation to obtain a mask video with an equivalent number of frames. c) The spatial dimension of the frames is reduced to $(h \times w) = (40 \times 100)$ to get better visuals of the fluid masks and reduce computation. d) Sliding-window method converts the mask video of dimensions $(D \times C \times h \times w) = (150 \times 1 \times 40 \times 100)$ to datapoints of dimensions $(n \times C \times d \times h \times w) = (138 \times 1 \times 12 \times 40 \times 100)$.

3.1 Fluid Masking

In order to isolate the fluid movement from other detectable features in the raw videos, we first trim the frames where the robot arm remains stationary after completing the shaking motion. We ensure that all trimmed videos within each dataset, both for classification and regression, maintain a consistent duration of 5 seconds, or 150 frames at 30 fps.

Next, we mask the fluid portion in the trimmed videos using the semantic segmentation model in S. Eppel et al. [30], which is a standard fully convolutional neural network trained through parsing the image into regions based on their class. To achieve better segmentation outputs, the model reduces the size of the RGB input videos from $(H \times W) = (1440 \times 1920)$ to (630×840) during inference. This masking process eliminates noise and unnecessary information, such as the RGB background or the arm motion from the raw video (Figure 2-a), allowing the spatio-temporal fluid oscillation to be the primary focus in the masked videos. Each masked frame is a binary, single-channel image with a pixel value of 1 indicating the fluid region (Figure 2-b).

To convert each binary mask video of dimensions $(D \times C \times H \times W) = (150 \times 1 \times 630 \times 840)$ into datapoints, we first resize the video and crop out the fluid regions obtaining $(D \times C \times h \times w) = (150 \times 1 \times 40 \times 100)$, where D is the number of frames in a mask video and h, w are the height and width of the cropped frames (Figure 2-c). Instead of generating non-overlapping splits of mask videos, we apply the sliding-window method with a window size of $d = 12$ frames, and stride of 1 over the first dimension to generate $(D - d)$ datapoints per video. Throughout this work, $D, d,$ and stride are

set to constants of 150, 12, and 1 respectively. Thus, each video is converted into datapoints of dimensions $(n \times c \times d \times h \times w) = (138 \times 1 \times 12 \times 40 \times 100)$, where each of the n datapoints consists of 12-frame clips from an original 150-frame mask video (Figure 2-d). This approach forms a denser training set that consists of $N(D - d)$ datapoints where N is the number of videos used to generate a dataset. Creating a large set of datapoints from each video is particularly beneficial in this work, considering the time-intensive nature of the physical video collection process. Each round of agitation and recording takes approximately 30-40 seconds, which makes the collection of a large number of videos impractical.

The **classification dataset** constructed from videos of five common fluids has 16,284 training and 4,140 testing datapoints extracted from 118 and 30 videos respectively. The **regression dataset** created from videos of glycerol solutions at eight different concentrations includes 27,600 training and 4,416 testing datapoints extracted from 200 and 32 videos respectively. Both the training sets are balanced with each type of sample having about 25 videos.

3.2 Autoencoder

Autoencoders (AEs) [45, 46] are a type of artificial neural network used to learn efficient latent representations of input data in a self-supervised manner. These latent representations are compact, encoded versions of the input data, and the learning process of an AE is based on minimizing the reconstruction error between the input data (which serves as the ground truth label) and the model's reconstructed output [46].

In the context of this work, we utilize the 3D convolutional AE, which can perform automatic feature detec-

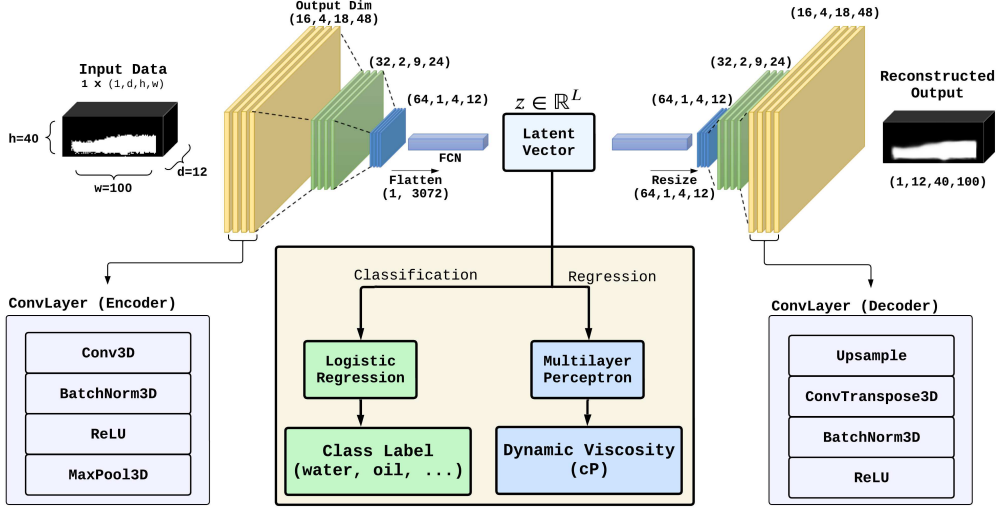


Figure 3: **Autoencoder Architecture and the Downstream Tasks.** The encoder (left) converts input datapoint of dimensions $(C \times d \times h \times w) = (1 \times 12 \times 40 \times 100)$ to a latent vector with dimension L , and the decoder (right) reconstructs the input data from the latent vector. For the classification task, logistic regression is applied to the sets of latent vectors to classify them and output a class label. For the viscosity regression task, a fully-connected network is attached to the encoder to output a viscosity prediction.

tion from video inputs and learn the spatio-temporal information by leveraging 3D convolutional layers [47, 48]. The latent representations generated by the encoder can be conveniently used for a variety of downstream tasks, specifically, fluid classification and viscosity regression.

Encoder. The encoder portion of the AE is composed of three convolutional layers, each of which includes a block of 3D convolution, batch normalization [49], ReLU activation [50], and max pooling operations with a $2 \times 2 \times 2$ kernel. The first convolutional layer uses a $5 \times 5 \times 5$ kernel while the subsequent two layers both use $3 \times 3 \times 3$ kernels. The number of kernels for each layers are 16, 32, and 64 respectively and the stride is constantly set to 1. The convolutional layers encode each input data of dimensions $1 \times 12 \times 40 \times 100$ into a reduced 3D representation of dimensions $64 \times 1 \times 4 \times 12$. An additional fully-connected network (FCN) after the convolution layers reduces the dimensionality of flattened 3D representations, 1×3072 , to a latent vector of dimension $1 \times L$ (we use $L = 512$).

Decoder. The decoder compartment begins with a FCN to expand the dimension of the latent vector back to a flattened 3D representation of 1×3072 . Each decoder layer includes upsampling layers with trilinear interpolation and transposed convolution to reconstruct the $1 \times 12 \times 40 \times 100$ mask frames from the unflattened 3D representations ($64 \times 1 \times 4 \times 12$), followed by batch normalization and ReLU activation. To ensure the output values fall within the range of 0 to 1, a sigmoid activation function was employed in the output layer, replacing the ReLU activation. Each of the three convolutional layers in the decoder uses 64 ($5 \times 5 \times 5$), 32 ($3 \times 3 \times 3$), and 16 ($3 \times 3 \times 3$) kernels respectively. This arrangement mirrors

the encoder’s structure and maintains a symmetric architecture within the autoencoder.

We pretrain a symmetric 3D convolutional AE by reconstructing the mask data and minimizing the MSE reconstruction loss (Figure 3). During training, we augment the input data with subtle translation and rotation transformations to enhance the model’s robustness to minor variations in the position and angle of the fluid masks caused by in-hand slippage or shaking of the workspace desk. We allow translations in the range of -2 to 3 pixels and rotations between -2 and 3 degrees.

To train each of the final classification and regression models, we use a latent dimension 512, and a batch size of 512. The Adam optimizer is used with a learning rate of $5e-5$ for classification and $7e-5$ for regression dataset, with a weight decay of $1e-5$ for both training instances. Each autoencoder is trained for 300 epochs.

3.3 Transfer Learning for Downstream Tasks

After training the AE on reconstructing oscillation patterns, we retain only the encoder, discarding the decoder. This approach utilizes the encoder’s ability to transform input data of shape $(C \times d \times h \times w) = (1 \times 12 \times 40 \times 100)$ into latent vectors, $z \in \mathbb{R}^L$.

For the classification task involving five categories of fluids, we apply multinomial logistic regression on sets of latent vectors. A classifier is fit with all 16,284 train latent vectors to provide a logistic regression model that outputs one-hot encoded class labels. Since each video is converted into multiple datapoints ($D - d$ for training and $D//d$ for inference without sliding-window), we select

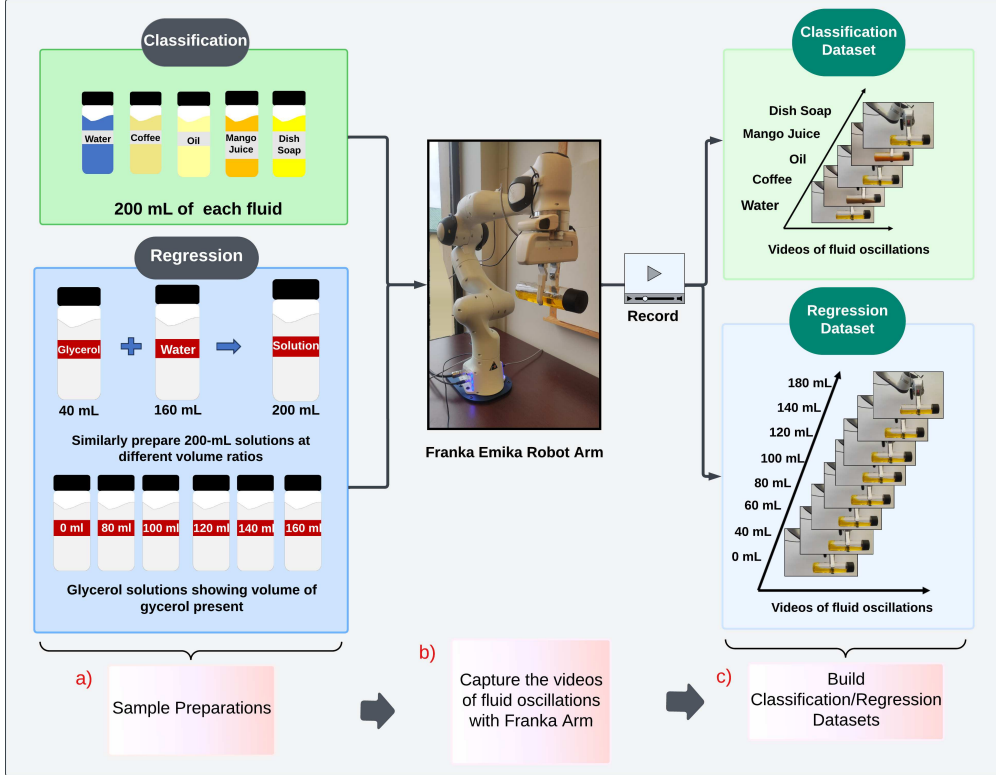


Figure 4: **Interactive Fluid Video Collection.** a) 200-mL common liquid samples are prepared to make the classification and regression datasets. b) Franka arm agitates the sample and the motion of fluid is recorded using a fixed position camera. Water and glycerol solution samples are dyed yellow to facilitate the semantic segmentation (Section 3.1).

the class that appears most frequently among all predictions to make a final class prediction at the video level.

For the viscosity regression task using the glycerol solutions, we attach an additional feed-forward MLP as a regression head and perform supervised learning with known viscosity labels obtained from [51]. The network is trained for 200 epochs with a learning rate of $3e-5$ and a batch size of 512, using the Adam optimizer to minimize the MSE loss between the predicted and actual viscosity values. To derive a final viscosity prediction at the video level, we average all viscosity predictions from each video.

4 Experimental Setup

Our experimental setup primarily involves a 7 DoF Franka Emika Panda robot arm, equipped with a gripper to hold and agitate the fluid container. We use cylindrical bottles of identical dimensions (20-cm length and 5-cm diameter) to hold each 200-mL fluid sample. We control the robot with Frankapy, a python wrapper for controlling the Franka arm [52].

To facilitate fluid semantic segmentation, we use a white cardboard background. In addition, given our focus on the effectiveness of segmented mask frames for under-

standing fluid properties, ensuring consistent mask quality across different fluid types is crucial. To this end, we dye transparent fluid samples, such as water and glycerol solutions, the same color. This ensures similar quality in the masks between fluid classes, to prevent the autoencoder from erroneously learning patterns in mask quality variation between classes, instead of oscillation patterns. In the future, this system could leverage a generative pipeline to transform all fluids to similar visual appearances before masking, similar to [41] to make this pipeline more generalizable.

4.1 Dataset Collection

Once the sample is positioned for interaction with the Franka Emika Panda robot arm (Figure 4-b), the robot applies a consistent lateral movement producing clear damped oscillation patterns in the sample. We maintain consistent force, arm trajectory, and bottle position during the shaking movement across all videos. This consistency isolates the features relevant to oscillation and prevents the model from learning irrelevant features, such as the relative positions of the bottle. We collect approximately 30 raw videos for each fluid sample using a camera attached to a fixed-position holder.

We establish separate video datasets for the classification and regression tasks. The classification dataset consists of

videos featuring different five fluids: coffee, dish soap, oil, fruit juice (mango), and water. For the regression dataset, we include videos of oscillating glycerol solutions at eight different concentrations, ranging from 0 to 90% by volume, with a total fluid volume of 200 mL. We choose glycerol for the regression dataset due to its wide viscosity range, from 1.0 (pure water) to about 250 centipoise (90 vol%) at 20 °C [51], which is significantly broader than that of comparable sucrose solutions. The videos were collected at constant frame rate of 30 fps and a resolution of $W \times H = 1920 \times 1440$. The data processing on raw videos can be found in Section 3.1.

5 Results

In this section, we first address the influence of segmentation quality on the overall predictive system. We then analyze the latent space of the pretrained AE using Principal Component Analysis (PCA) for 2D visualization [42]. For the classification task involving five fluid categories, we present the classification accuracy computed on each video by comparing the class predictions to labels. This is followed by an evaluation of the accuracy across all 30 test classification videos. For the regression task, which requires an additional training of a fully-connected network, we present an ablation study under three common training configurations: freezing the pretrained parameters, not freezing the pretrained parameters, and not pretraining at all.

5.1 Segmentation Quality

The mask videos obtained using the pretrained semantic segmentation model from [30] successfully capture the frame level oscillations of fluid (Figure 5-a). In order to use these masks as visual features for differentiating fluid categories or predicting the viscosity of the fluid, it is important to ensure consistent mask quality across different fluid types. This is because the model predictions should be based solely on the oscillation patterns of the fluid, not on other factors such as the shape of the segmented masks, their positions, or any artifacts created by the segmentation process. For instance, as shown in Figure 5-a, segmented masks on fluid are sometimes discontinuous because the model misclassifies fluid as the part of robot’s gripper.

Another challenge in providing consistent masks is in the nature of the Vector Lab-Pics training data used to provide the pretrained segmentation model [30]. The model was primarily trained on images of transparent fluids and solid materials, which can lead to poor segmentation performance when applied to opaque fluids such as syrup and coffee. The quality of the masks not only depends on the color of the fluid but also depends on the lighting condition of the workspace and the camera angle. Inconsistent or imperfect mask qualities can cause the model to overfit to the masking discrepancies, rather than learning based on the oscillation patterns. To address this problem,

we collect the videos under strict lighting conditions and maintain a consistent camera angle throughout the video collection process; further details on data collection are found in Figure 4. This ensures that the variations in mask quality are minimized and the model can focus on learning the oscillation patterns of the fluid.

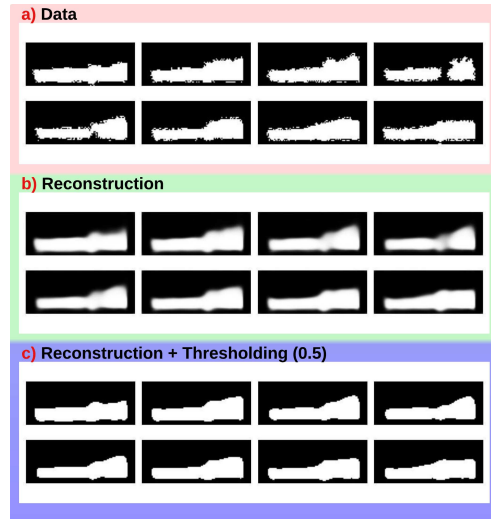


Figure 5: **Example Segmentation Masks and Autoencoder Reconstruction Output.** a) The mask frames obtained from the segmentation model are processed as shown in Section 3.1. The discontinuity observed in the fluid mask is due to incorrect segmentation. b) The autoencoder is pretrained through a reconstruction task. c) Pixel values are thresholded to produce binary frames, closely resembling the input data.

5.2 Latent Space Analysis

To gain a deeper understanding of our autoencoder’s learning dynamics, we utilize PCA to reduce the dimensionality of the latent representations and visualize them in 2D plane. This allows us to visually inspect the distribution and relationships between the encoded datapoints. A previous work [42] demonstrates the capability of Video-Specific Autoencoders to learn a temporally continuous representations without any explicit temporal information. Similarly, in this work, we observe that each encoded video forms a continuous trajectory within this PCA space, despite the absence of explicit temporal information (Figure 6-c). Furthermore, we observe that the trajectories from different videos exhibit a similar direction and shape, often resembling ‘U’ or ‘W’ shape (Figure 7), potentially because the videos were taken under a strict laboratory setup. Given that video autoencoders can learn the repetitive motion present in a video [42], we find that datapoints consisting of earlier frames with more intense oscillation patterns (Datapoints 1-3 in Figure 6-c) are located close to each other in the PCA space. Conversely, datapoints containing the later oscillations in the video, where significant decay of oscillation has taken place, are clustered together but located far from the earlier datapoints (Datapoints 136-138). When the training

of the autoencoder is augmented with translation and rotation, the trajectories form relatively more complex curves, similar to formation of *distinct modes* in [42], compared to training without any augmentation.

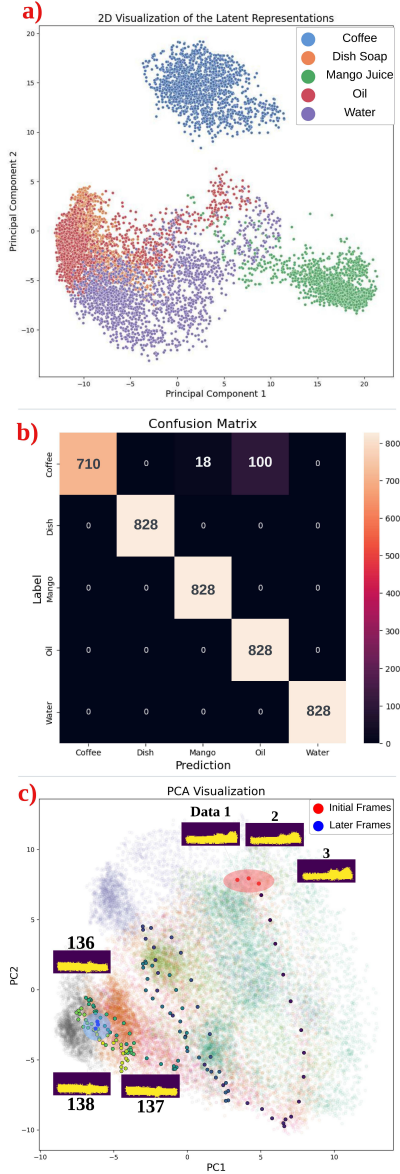


Figure 6: **a)** 2D PCA visualization of encoded classification dataset with 5 categories shown at the right-top of the plot. **b)** Classification Confusion Matrix obtained from Logistic Regression; 16,284 latent vectors from the train set and making prediction on 4,140 test set latent vectors. Total of 103 datapoints representing coffee are misclassified as either mango juice or oil. **c)** PCA visualization of a single-video trajectory ($50\text{vol}\%$ glycerol solution) within the encoded regression dataset. Each point in the PCA spaces (**a,b**) represent an encoded representation of the $1 \times 12 \times 40 \times 100$ datapoint.

5.3 Classification

In this section, we present our results on classifying fluid categories present in each of the videos in the classification test dataset (Section 3.1). We utilize multinomial logistic regression to classify the latent vectors encoded with the pretrained autoencoder. Within the 2D latent representations (Figure 6-a), each fluid class forms a distinct cluster. This observation suggests that the latent vectors, with a dimensionality of $L = 512$, provide a suitable basis for classification tasks.

Among the 4,140 test datapoints from a total of 30 test videos, we reserve 6 videos for each class, or $138 * 6 = 828$ datapoints as illustrated in the confusion matrix (Figure 6-b). To make class predictions at test time, our model classifies each datapoint for a singular video, and the video-level prediction is set to the class with the greatest number of datapoint-level predictions. The classification model (Encoder and Logistic Regression) achieves an overall accuracy of **97.5%**, resulting in 103 misclassifications out of the 4,140 datapoints. These incorrect classifications are from a specific video of the coffee class, potentially due to the quality of the segmentation masks (Section 5.1). On a video level, the model achieves prediction accuracy of **96.6%**, correctly classifying 29 out of 30 videos.

5.4 Regression

In our approach, we generate a single viscosity value for each input mask datapoint in the regression test dataset by employing a separate fully-connected network (FCN) that leverages the encoder portion of the AE (Figure 3). In order to compare various training methodologies, we conduct an ablation study on the encoder weights. We first train the FCN with the encoder parameters frozen maintaining the pretrained weights. We then train it with the encoder parameters unfrozen, allowing the encoder weights to be fine-tuned during the FCN training. Lastly, we train the network directly for the downstream regression task without any pretraining the encoder.

Table 1: **Mean Absolute Errors for Different MLP Training Methods.** The model pretrained with unfrozen encoder parameters performs the best in terms of MAE computed between the predicted viscosities and labels in centipoise (cP). Exceptionally high MAE for the unpretrained model compared to other two demonstrates the effectiveness of the pretraining process.

Method	MAE
Pretraining with frozen encoder parameters	1.955
Pretraining with unfrozen encoder parameters	0.258
No Pretraining	17.881

The performance of the regression model (Encoder and MLP) is assessed based on the mean absolute error computed across all 4,416 test prediction-label pairs (Table 1). The significantly higher MAE (approximately 18 cP) observed for the model without pretraining compared to

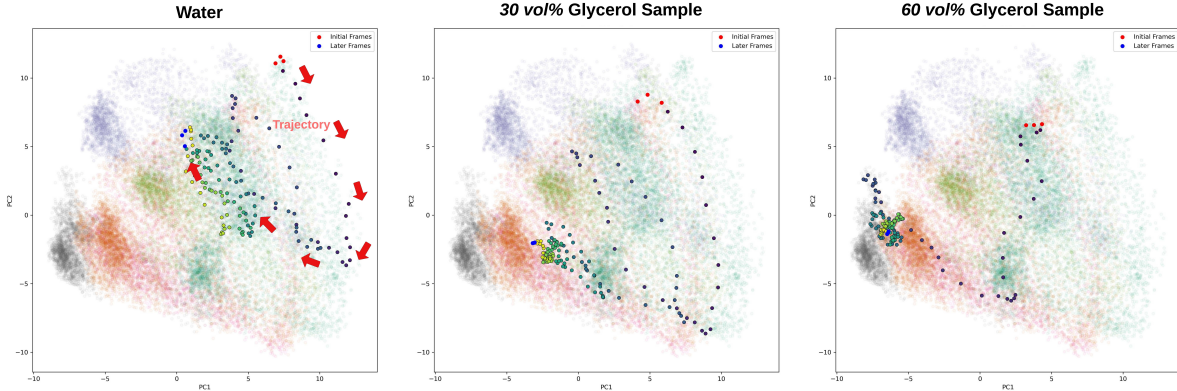


Figure 7: **Trajectories for Different Fluid Samples.** Pure water (left), 30 vol % (middle), and 60 vol % (right) glycerol solutions are projected on the 2D PCA space for visualization. In the left image, direction of the trajectory is shown with a sequence of red arrows. Trajectory for the 30 vol % glycerol sample is more irregular compared to others. This could be attributed to random augmentation applied during the training.

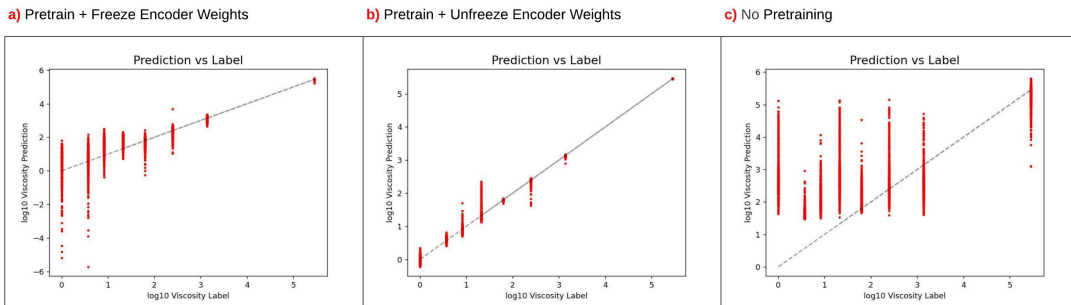


Figure 8: **Comparison of Predicted Viscosity and Ground Truth.** The viscosity predictions are plotted against the ground truth labels in \log_{10} space for improved visibility. The regression model in (b) yields the lowest MAE among the three training methods, indicating superior performance among the three models.

the pretrained models suggests that pretraining is crucial in enhancing the overall performance of the regression model. It can also be observed that unfreezing the encoder parameters can further minimize the loss compared to training with frozen weights. In addition, unfreezing the encoder weights leads to improved performance, which can be visually confirmed in Figure 8 by the reduced variance in the predictions from the model trained with unfrozen encoder weights.

6 Limitations and Future Work

In this work we present a novel interactive perception approach to predicting fluid viscosity purely from visual observation. While we have demonstrated the effectiveness of this method, there are some key limitations that if addressed could result in further improvements, specifically the segmentation mask quality and the generalizability. In this work, we directly leverage the segmentation model

from [30]; however, these segmentation masks can be noisy, introducing more error into the system. Developing a more reliable liquid segmentation module could further improve the pipeline. Furthermore, we collect the dataset under strict conditions to ensure limited variation in lighting conditions, robot movement, etc. A more generalizable extension to this existing work would be to collect a larger dataset with variation across lighting conditions, robot sloshing force, etc. to ensure robust prediction with more variation in the data collection environment. Beyond fluid property prediction, we hope to combine this interactive perception module with more complex fluid handling tasks, such that the robot has a container of unidentified fluid, leverages this pipeline to intuit the viscosity, and uses the predicted viscosity to inform the control of a pouring, stirring, or sloshing task.

Data availability

All codes used for processing the collected videos and training models are available at GitHub (<https://github.com/BaratiLab/vid2visc>). The Segmentation folder contains the modified code for pretrained model based on the previous work of S. Eppel et al. [30] An example of segmented outputs (.avi) for each fluid sample is included in folders classification_dataset and regression_dataset. The folder autoencoder contains the python codes for training and the two downstream tasks. All RGB videos and segmented videos used to make the classification and regression dataset can be found in a public Google Drive (.zip).

Acknowledgements

This work is supported by the Department of Mechanical Engineering, Carnegie Mellon University, United States. The authors would like to thank our Lab Instructor M. Cline for providing access to the chemistry laboratory facilities and supplying the necessary materials for solution preparation.

References

- [1] Xiaodong Gao, Pingchuan Dong, Jiawei Cui, and Qichao Gao. Prediction model for the viscosity of heavy oil diluted with light oil using machine learning techniques. *Energies*, 15(6), 2022.
- [2] Sudhanshu Tiwari, Ajay Dangi, and Rudra Pratap. A tip-coupled, two-cantilever, non-resonant microsystem for direct measurement of liquid viscosity. *Microsystems & nanoengineering*, 9:34, 03 2023.
- [3] Rouhollah Torabi and Seyyed Nourbakhsh. The effect of viscosity on performance of a low specific speed centrifugal pump. *International Journal of Rotating Machinery*, 2016:1–9, 01 2016.
- [4] Arnold J. T. M. Mathijssen, Maciej Lisicki, Vivek N. Prakash, and Endre J. L. Mossige. Culinary fluid mechanics and other currents in food science. *Reviews of Modern Physics*, 95(2), jun 2023.
- [5] Naruki Yoshikawa, Andrew Zou Li, Kourosh Darvish, Yuchi Zhao, Haoping Xu, Artur Kuramshin, Alán Aspuru-Guzik, Animesh Garg, and Florian Shkurti. Chemistry lab automation via constrained task and motion planning, 2023.
- [6] Benjamin Burger, Phillip Maffettone, Vladimir Gusev, Catherine Aitchison, Yang Bai, Xiaoyan Wang, Xiaobo Li, Ben Alston, Buyi Li, Rob Clowes, Nicola Rankin, Brandon Harris, Reiner Sprick, and Andrew Cooper. A mobile robotic chemist. *Nature*, 583:237–241, 07 2020.
- [7] Hatem Fakhrudeen, Gabriella Pizzuto, Jakob Glowacki, and Andrew Ian Cooper. Archemist: Autonomous robotic chemistry system architecture, 2022.
- [8] Aaron Butterworth, Gabriella Pizzuto, Leszek Pecyna, Andrew I. Cooper, and Shan Luo. Leveraging multi-modal sensing for robotic insertion tasks in r & d laboratories, 2023.
- [9] Parisa Shiri, Veronica Lai, Tara Zepel, Daniel Griffin, Jonathan Reifman, Sean Clark, Shad Grunert, Lars Yunker, Sebastian Steiner, Henry Situ, Fan Yang, Paloma Prieto, and Jason Hein. Automated solubility screening platform using computer vision. *iScience*, 24:102176, 02 2021.
- [10] Hung-Jui Huang, Xiaofeng Guo, and Wenzhen Yuan. Understanding dynamic tactile sensing for liquid property estimation. *arXiv preprint arXiv:2205.08771*, 2022.
- [11] Michael Sinhuber, Eberhard Bodenschatz, and Gregory P. Bewley. Decay of turbulence at high reynolds numbers. *Phys. Rev. Lett.*, 114:034501, Jan 2015.
- [12] Jan Assen, Shin’ya Nishida, and Roland Fleming. Visual perception of liquids: Insights from deep neural networks. *PLOS Computational Biology*, 16:e1008018, 08 2020.
- [13] Carolyn Matl. *Interactive Perception for Robotic Manipulation of Liquids, Grains, and Doughs*. PhD thesis, EECS Department, University of California, Berkeley, Aug 2021.
- [14] Jeannette Bohg, Karol Hausman, Bharath Sankaran, Oliver Brock, Danica Kragic, Stefan Schaal, and Gaurav S. Sukhatme. Interactive perception: Leveraging action in perception and perception in action. *IEEE Transactions on Robotics*, 33(6):1273–1291, dec 2017.
- [15] Lin Shao, Parth Shah, Vikranth Dwaracherla, and Jeannette Bohg. Motion-based object segmentation based on dense RGB-d scene flow. *IEEE Robotics and Automation Letters*, 3(4):3797–3804, oct 2018.
- [16] Zijie Li and Amir Barati Farimani. Graph neural network-accelerated lagrangian fluid simulation. *Computers & Graphics*, 103:201–211, 2022.
- [17] Connor Schenck and Dieter Fox. Spnets: Differentiable fluid dynamics for deep neural networks. In Aude Billard, Anca Dragan, Jan Peters, and Jun Morimoto, editors, *Proceedings of The 2nd Conference on Robot Learning*, volume 87 of *Proceedings of Machine Learning Research*, pages 317–335. PMLR, 29–31 Oct 2018.
- [18] Dule Shu, Zijie Li, and Amir Barati Farimani. A physics-informed diffusion model for high-fidelity flow field reconstruction. *Journal of Computational Physics*, 478:111972, 2023.
- [19] Ricardo Vinuesa and Steven L Brunton. Enhancing computational fluid dynamics with machine learning. *Nature Computational Science*, 2(6):358–366, 2022.
- [20] Zherong Pan, Chonhyon Park, and Dinesh Manocha. Robot motion planning for pouring liquids. In *Proceedings of the international conference on automated planning and scheduling*, volume 26, pages 518–526, 2016.
- [21] Tatiana López Guevara, Nicholas Kenelm Taylor, Michael Gutmann, Subramanian Ramamoorthy, and Kartic Subr. Adaptable pouring: Teaching robots not to spill using fast but approximate fluid simulation. In *1st Conference on Robot Learning 2017*, pages 77–86, 2017.
- [22] Monroe Kennedy, Kendall Queen, Dinesh Thakur, Kostas Daniilidis, and Vijay Kumar. Precise dispensing of liquids using visual feedback. In *2017 IEEE/RSJ international conference on intelligent robots and systems (IROS)*, pages 1260–1266. IEEE, 2017.
- [23] Monroe Kennedy, Karl Schmeckpeper, Dinesh Thakur, Chenfanfu Jiang, Vijay Kumar, and Kostas Daniilidis. Autonomous precision pouring from unknown containers. *IEEE Robotics and Automation Letters*, 4(3):2317–2324, 2019.
- [24] Zhou Xian, Bo Zhu, Zhenjia Xu, Hsiao-Yu Tung, Antonio Torralba, Katerina Fragkiadaki, and Chuang Gan. Fluidlab: A differentiable environment for benchmarking complex fluid manipulation. *arXiv preprint arXiv:2303.02346*, 2023.
- [25] Gheorghe Lisca, Daniel Nyga, Ferenc Bálint-Benczédi, Hagen Langer, and Michael Beetz. Towards robots conducting chemical experiments. In *2015 IEEE/RSJ International Conference on Intelligent Robots and Systems (IROS)*, pages 5202–5208. IEEE, 2015.
- [26] Benjamin Burger, Phillip M Maffettone, Vladimir V Gusev, Catherine M Aitchison, Yang Bai, Xiaoyan Wang, Xiaobo Li, Ben M Alston, Buyi Li, Rob Clowes, et al. A mobile robotic chemist. *Nature*, 583(7815):237–241, 2020.
- [27] Naruki Yoshikawa, Andrew Zou Li, Kourosh Darvish, Yuchi Zhao, Haoping Xu, Alan Aspuru-Guzik, Animesh Garg, and Florian Shkurti. An adaptive robotics framework for chemistry lab automation. *arXiv preprint arXiv:2212.09672*, 2022.
- [28] Pranshu Pant, Ruchit Doshi, Pranav Bahl, and Amir Barati Farimani. Deep learning for reduced order modelling and efficient temporal evolution of fluid simulations. *Physics of Fluids*, 33(10), 2021.
- [29] Hamidreza Eivazi and Ricardo Vinuesa. Physics-informed deep-learning applications to experimental fluid mechanics, 2022.
- [30] Sagi Eppel, Haoping Xu, and Alán Aspuru-Guzik. Computer vision for liquid samples in hospitals and medical labs using hierarchical image segmentation and relations prediction. *CoRR*, abs/2105.01456, 2021.
- [31] Karol Hausman, Scott Niekum, Sarah Osentoski, and Gaurav S Sukhatme. Active articulation model estimation through interactive perception. In *2015 IEEE International Conference on Robotics and Automation (ICRA)*, pages 3305–3312. IEEE, 2015.

- [32] Manuel Baum, Matthew Bernstein, Roberto Martin-Martin, Sebastian Höfer, Johannes Kulick, Marc Toussaint, Alex Kacelnik, and Oliver Brock. Opening a lockbox through physical exploration. In *2017 IEEE-RAS 17th International Conference on Humanoid Robotics (Humanoids)*, pages 461–467. IEEE, 2017.
- [33] Michelle A. Lee, Yuke Zhu, Peter Zachares, Matthew Tan, Krishnan Srinivasan, Silvio Savarese, Li Fei-Fei, Animesh Garg, and Jeannette Bohg. Making sense of vision and touch: Learning multimodal representations for contact-rich tasks, 2019.
- [34] Lin Shao, Toki Migimatsu, and Jeannette Bohg. Learning to scaffold the development of robotic manipulation skills, 2020.
- [35] Santhosh Kv and Vignesh Shenoy. Analysis of liquid viscosity by image processing techniques. *Indian Journal of Science and Technology*, 9, 08 2016.
- [36] Wenzhen Yuan, Siyuan Dong, and Edward H Adelson. Gelsight: High-resolution robot tactile sensors for estimating geometry and force. *Sensors*, 17(12):2762, 2017.
- [37] Enze Xie, Wenjia Wang, Wenhai Wang, Mingyu Ding, Chunhua Shen, and Ping Luo. Segmenting transparent objects in the wild. In *Computer Vision—ECCV 2020: 16th European Conference, Glasgow, UK, August 23–28, 2020, Proceedings, Part XIII 16*, pages 696–711. Springer, 2020.
- [38] Jie Liao, Yanping Fu, Qingan Yan, and Chunxia Xiao. Transparent object segmentation from casually captured videos. *Computer Animation and Virtual Worlds*, 31(4-5):e1950, 2020.
- [39] Akihiko Yamaguchi and Christopher G. Atkeson. Stereo vision of liquid and particle flow for robot pouring. In *2016 IEEE-RAS 16th International Conference on Humanoid Robots (Humanoids)*, pages 1173–1180, 2016.
- [40] Connor Schenck and Dieter Fox. Visual closed-loop control for pouring liquids, 2017.
- [41] Gautham Narayan Narasimhan, Kai Zhang, Ben Eisner, Xingyu Lin, and David Held. Self-supervised transparent liquid segmentation for robotic pouring, 2022.
- [42] Kevin Wang, Deva Ramanan, and Aayush Bansal. Video exploration via video-specific autoencoders. *CoRR*, abs/2103.17261, 2021.
- [43] Zihang Lai, Sifei Liu, Alexei A. Efros, and Xiaolong Wang. Video autoencoder: self-supervised disentanglement of static 3d structure and motion, 2021.
- [44] Yunpeng Chang, Zhigang Tu, Wei Xie, and Junsong Yuan. Clustering driven deep autoencoder for video anomaly detection. In *Computer Vision—ECCV 2020: 16th European Conference, Glasgow, UK, August 23–28, 2020, Proceedings, Part XV 16*, pages 329–345. Springer, 2020.
- [45] Ian J. Goodfellow, Yoshua Bengio, and Aaron Courville. *Deep Learning*. MIT Press, Cambridge, MA, USA, 2016. <http://www.deeplearningbook.org>.
- [46] Yoshua Bengio, Aaron Courville, and Pascal Vincent. Representation learning: A review and new perspectives, 2014.
- [47] Hiroyuki Yamaguchi, Yuki Hashimoto, Genichi Sugihara, Jun Miyata, Toshiya Murai, Hidehiko Takahashi, Manabu Honda, Akitoyo Hishimoto, and Yuichi Yamashita. Three-dimensional convolutional autoencoder extracts features of structural brain images with a “diagnostic label-free” approach: Application to schizophrenia datasets. *Frontiers in Neuroscience*, 15, 2021.
- [48] Ali Mjalled, Reza Namdar, Lucas Reineking, Mohammad Norouzi, Fathollah Varnik, and Martin Mönnigmann. Parametric 3d convolutional autoencoder for the prediction of flow fields in a bed configuration of hot particles, 2023.
- [49] Sergey Ioffe and Christian Szegedy. Batch normalization: Accelerating deep network training by reducing internal covariate shift, 2015.
- [50] Alex Krizhevsky, Ilya Sutskever, and Geoffrey Hinton. Imagenet classification with deep convolutional neural networks. *Neural Information Processing Systems*, 25, 01 2012.
- [51] John Bartlett Segur and Helen E. Oberstar. Viscosity of glycerol and its aqueous solutions. *Industrial & Engineering Chemistry*, 43:2117–2120, 1951.
- [52] Kevin Zhang, Mohit Sharma, Jacky Liang, and Oliver Kroemer. A modular robotic arm control stack for research: Franka-interface and frankapy. *arXiv preprint arXiv:2011.02398*, 2020.